Colloids and Surfaces A 600 (2020) 124943

Contents lists available at ScienceDirect

Colloids and Surfaces A

journal homepage: www.elsevier.com/locate/colsurfa

Engineering nanocellulose superabsorbent structure by controlling the drying rate

Ruth M. Barajas-Ledesma[a], Antonio F. Patti[b], Vanessa N.L. Wong[c], Vikram Singh Raghuwanshi[a], Gil Garnier[a,*]

[a] Bioresource Processing Research Institute of Australia (BioPRIA) and Department of Chemical Engineering, Monash University, Clayton, VIC 3800, Australia
[b] School of Chemistry, Monash University, Clayton, VIC 3800, Australia
[c] School of Earth, Atmosphere & Environment, Monash University, Clayton, VIC 3800, Australia

GRAPHICAL ABSTRACT

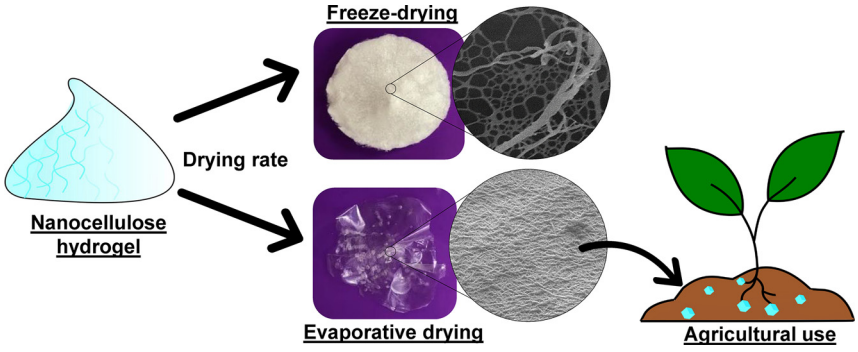

ARTICLE INFO

Keywords:
Superabsorbent
TEMPO-mediated oxidation
Nanocellulose
Structure
Drying
Hornification

ABSTRACT

Hypothesis: The absorption performance and structure of superabsorbents prepared from carboxylated nanocellulose are strongly influenced by the rate of water removal. Their structure can be engineered by changing the drying profile.

Experiments: TEMPO-oxidised nanocellulose superabsorbents were prepared using five different drying techniques, each providing a distinct drying rate. The absorption capacity of deionised water was measured as a function of time and the swelling kinetics was determined, modelled and related to the superabsorbent structure. Superabsorbent phytotoxicity was assessed through seed emergence tests.

Findings: The absorption performance of nanocellulose superabsorbents is controlled by the drying rate. In most cases, drying the nanocellulose superabsorbents via evaporation increases the absorption capacity compared to freeze-dried superabsorbents. The best nanocellulose superabsorbent was the air-dried, absorbing around 230 g water/g dry fibre. The high absorption capacity of the evaporative dried superabsorbents is due to their high pore area which increases the interaction between water molecules and fibres. This leads to a stronger physical entrapment of water by capillary forces. Seed germination studies demonstrated that oven-dried 50 °C superabsorbent increased germination by 40 %. Carboxylated nanocellulose superabsorbents emerge as high-performance renewable materials which can be used extensively in many applications, including agriculture.

* Corresponding author.
E-mail address: Gil.Garnier@Monash.edu (G. Garnier).

https://doi.org/10.1016/j.colsurfa.2020.124943
Received 6 April 2020; Received in revised form 30 April 2020; Accepted 1 May 2020
Available online 06 May 2020

1. Introduction

Superabsorbent polymers (SAPs) are physically or chemically cross-linked three-dimensional (3D) networks made of linear or branched hydrophilic polymers [1]. Superabsorbents can absorb water or fluids at hundreds of times their own weight and remain stable in the swollen state [1–4]. The degree of swelling is governed by the mobility of ions from the external solution toward the centre of the superabsorbent, also known as counter-ion entropy, that induces an osmotic pressure difference across the material network [5,6]. Superabsorbents have been used in many applications including biomedicine [5], food and beverages [7], personal care and hygiene products [8], soil remediation and wastewater treatment [9] and agriculture [10]. In agriculture, SAPs can ameliorate water availability for plants [11]. These serve as soil conditioners, improving soil properties, reducing the irrigation water consumption, and increasing crop yield [12,13], and as nutrient carriers [13].

Most of the commercial superabsorbents are synthetic polymers, such as polyacrylamides or polyacrylates, which are non-biodegradable. Growing environmental and health concerns have driven the search for natural polymer-based superabsorbents, especially those made of polysaccharides, such as pectin or starch [14,15]. Cellulose, the most abundant polymer on earth, has also been investigated as a superabsorbent for its availability, low-cost, biodegradability, renewability and hydrophilicity [13,16]. Different synthesis methods have been examined to produce cellulose-based SAPs [17]. Among those, the TEMPO-mediation oxidation of cellulose is currently considered one of the most effective method for producing nanocellulose-based SAPs [6,18]. This process oxidises the easily accessible primary alcohol groups (C6) to the carboxylic acid, resulting in a cellulose structure containing some C6 carbons in carboxylic acid form. This surface modification provides the necessary electrostatic repulsion which assists the liberation of nanocellulose fibres upon mechanical fibrillation [19]. The resulting material, also referred to as hydrogel, consists of an entanglement of cellulose nanofibres (CNF) creating a porous material of high specific surface area [20]. Several reviews about nanocellulose-based material properties, production, structure and applications have been published [17,20–22].

A major challenge in the production of nanocellulose-based superabsorbents is to retain their porous structure during water removal. Different drying rates determined by the drying process have been examined to remove the water from hydrogels. Among these, freeze-drying has become the preferred method for laboratory preparation of highly-porous, ultralow-density solid SAPs of high water retention and swelling properties [20,23]. These are commonly known as foams or aerogels [20]. Freezing followed by sublimation of ice prevents the formation of capillary pressure, preserving the structure of the original dispersion. However, freeze-drying is not only expensive and difficult to perform on a large-scale [23], but it also produces low-density and fast swelling superabsorbent of limited application range. In agriculture, for example, a fast swelling rate can selectively sequester water, thus restricting the water availability to plants creating an undesirable water stress environment [12]. Thus, controlling the superabsorbent properties and structure which affect plant growth is crucial.

Evaporative-drying presents an alternative. Buchtová and Budtova [24] reported the evaporative vacuum drying at room temperature of microcrystalline cellulose dissolved in ionic liquids to produce superabsorbents with a volume shrinkage of 90 %, very low porosity and no measurable surface area because of the collapse of the porous polymer network. Beaumont et al. [25] compared the effects of oven-drying at 60 °C and freeze-drying on the redispersibility of TENCEL gel, composed of spherical cellulose II microparticles. Surprisingly, they showed that oven-dried superabsorbents had better colloidal stability and higher water retention than freeze-dried superabsorbents. This was attributed to the low process temperatures and superabsorbent additives, such as carboxylmethylcellulose, that minimises the agglomeration and collapse of fibres during drying, referred to as hornification [26]. Hornification can also be minimised by preparing superabsorbents at high pH or by carboxylation of cellulose; a high-density of dissociated carboxylic groups prevents agglomeration by electrostatic stabilization [22,27].

While several studies have investigated the synthesis and formulation of cellulose-based superabsorbents, none have systematically compared the effect of drying rate and profile on the structure of nanocellulose superabsorbents nor related those to the absorption capacity and swelling kinetics. The effect of the drying rate on the morphology, porosity and pore properties of nanocellulose superabsorbent and how these properties influence plant growth remains poorly understood.

In this study, carboxylated nanocellulose hydrogels were prepared via TEMPO oxidation followed by high-pressure homogenization. This standard carboxylated nanocellulose hydrogel was dried to create a superabsorbent using five different drying techniques, each providing a different drying rate: freeze-drying, air-drying, vacuum drying, and oven-drying at high and low temperature. The superabsorbent absorption properties and the swelling kinetics were quantified. It is our objective to analyse the effect that drying rate has on the resulting superabsorbent structure and to establish the relationship with its absorption characteristics. Of special interest is the production of cellulose-based superabsorbents as hydro-retentor materials for applications in sustainable agriculture.

2. Materials and methods

2.1. Materials

Bleached Eucalyptus Kraft (BEK) pulp, containing around 90 % w/w of moisture was provided by Australian Paper, Maryvale, Australia. The chemical composition of the BEK pulp is displayed in Table 1 [28]. 2,2,6,6-Tetramethylpiperidine-1-oxyl (TEMPO) and sodium bromide (NaBr) were purchased from Sigma-Aldrich. Sodium hydroxide (NaOH) and hydrochloric acid (HCl) were diluted for solutions as required and purchased from Merck and ACL Laboratories, respectively. 12 % w/v sodium hypochlorite (NaClO) was purchased from Thermo Fisher Scientific and used as received. Radish (*Raphanus Sativus*) and cress (*Lepidium sativum L.*) seeds were purchased from Mr. Fothergill's (South Windsor, Australia).

2.2. Superabsorbent preparation

Nanocellulose superabsorbent was prepared following the TEMPO-mediated oxidation process developed by Isogai et al. [19]. Briefly, 25 g (dry weight) of BEK pulp was suspended in 2500 mL of water containing 0.4 g and 2.5 g of dissolved TEMPO and NaBr, respectively. The 12 % w/v NaClO was initially adjusted to pH 10 through addition of 36 % w/v HCl. The oxidation process started by adding 100 mL NaClO (6.6 mmol NaClO/g cellulose) drop-wise to the suspension under constant stirring. The pH of the reaction was kept at 10 via addition of 0.5 M NaOH. The reaction was maintained for 3 h or until no decrease in pH was observed. The oxidised fibres were washed with deionised water, recovered by filtration. The TEMPO-oxidised cellulose had a carboxylate content of 1.4 mmol/g as determined by conductivity

Table I
Chemical composition of BEK pulp in dry basis.

Chemical composition	Average content (% ± standard deviation)
Cellulose	78.7 ± 0.8
Hemicellulose	17.7 ± 0.4
Lignin	3.2 ± 0.1
Extractives	0.3 ± 0.1
Ash	0.2 ± 0.1

titration [29].

The TEMPO-oxidised cellulose was then dispersed in deionised water to achieve a concentration of 0.5 % w/v. Fibrillation was accomplished by using a high-pressure homogeniser (GEA Niro Soavi Homogeniser Panda) at 1000 bar and two passes.

After fibrillation, five drying techniques were employed to produce the superabsorbent: freeze-drying, air-drying, vacuum-drying at 50 °C and oven-drying at 50 °C and 105 °C. Freeze-dried nanocellulose superabsorbent was prepared by freezing the nanocellulose samples for at least 12 h at −80 °C. Once frozen, samples were freeze-dried (Christ Alpha 2-4 LD Plus) for 2 days. Air-dried samples were allowed to dry at ambient temperature (approx. 23 °C) until no difference in mass was observed. Vacuum oven-dried nanocellulose samples were prepared by drying in a vacuum oven (Thermoline Scientific Vacuum drying oven) at 50 °C until no difference in mass was observed. Oven-dried nanocellulose samples were prepared by drying in an oven at either 50 °C or 105 °C until no difference in mass was observed.

2.3. Characterisation

The structural morphology of all superabsorbents was analysed by SEM using a FEI Nova NanoSEM and a FEI Magellan 400. Samples were mounted on a metal stub coated with an Iridium layer less than 2 nm thick. Micrographs were obtained in high vacuum-mode.

The pore size distribution, porosity (total and at P = 1 atm) and pore surface of all samples were determined by mercury porosimetry (Micromeritics Autopore IV). Samples were degassed at 50 °C for at least 24 h prior testing. Two replicates per sample were conducted. In all measurements, the contact angle at the Hg-sample interface was assumed to be 130° and a testing pressure range from 0.1 to 60,000 psia was applied. The desired values were obtained through the Washburn Equation:

$$D = \frac{-4\gamma cos\theta}{P} \quad (1)$$

where D is the pore diameter, γ is the surface tension of mercury, θ refers to the contact angle between the mercury and the pore wall, and P is the applied pressure.

SAXS measurements were performed at the X-ray facility lab, Monash University with a Bruker N8 Horizon instrument using a CuKα (λ = 1.54 Å) micro-source. The sample to detector distance was 0.6 m which covers the q range between ~0.015 to 0.3 $Å^{-1}$. The scattered photons from the sample were collected on a 2D Vantec-500 detector (pixel size ~70 µm × 70 µm). Final scattering curves were obtained by radial averaging of scattering images with the Bruker EVA software.

2.4. Swelling and water retention studies

The swelling capacity of the superabsorbents prepared was evaluated in deionised water. Both swelling capacity and swelling rate were measured. The swelling capacity was determined by weighing the samples before and after immersion in deionised water for at least 24 h. The swelling capacity was calculated as follows:

$$Swelling\ capacity,\ Q = \frac{m_t - m_d}{m_d} \quad (2)$$

where m_t is the weight of the swollen superabsorbent at time t and m_d refers to the weight of the dried sample.

The swelling rate was evaluated by monitoring the weight gain of the samples after immersion in water over different periods of time and expressed as Q variations. Results are reported as the average and standard deviation of triplicates.

The water retention value (WRV) of all rehydrated superabsorbents was performed in triplicates following ISO 17190-6 [30]. The set up was adapted from Qingzheng Cheng [31]. Briefly, superabsorbent samples were immersed in deionised water for at least 48 h prior to testing. Each wet sample was placed in a polypropylene mesh placed inside empty centrifugation tubes (supplementary information, S1). Centrifugation was carried out 3 min at a relative centrifugal force (RCF) of 250 G at room temperature. After centrifugation, the "wet weight" of the samples was measured. The samples were oven dried at 105 °C until they reached constant mass. The WRV was calculated as follows:

$$WRV = \frac{m_c - m_d}{m_d} \quad (3)$$

where m_c is the weight of the wet sample after centrifugation and m_d refers to the weight of the dry sample.

2.5. Seed germination tests

The impact of the superabsorbents, freeze-dried and oven-dried 50 °C, on the germination and growth of two plant species was assessed. The species selected were radish and cress.

Superabsorbent effects on seed germination were evaluated at concentrations of 2, 5, 10 g of superabsorbent/L. The application rate was within the recommended range for commercial superabsorbents [32]. For each treatment, different amounts of the nanocellulose before drying were spread on a filter paper according to the desired concentration. The filter paper was later freeze-dried or oven-dried at 50 °C, assuring even distribution of the superabsorbent on the filter paper. Once dried, the filter paper with the superabsorbent was placed in a 90 mm Petri dish and 5 mL of deionised water was poured. After the addition of water, 10 seeds of each species were placed on the wetted filter paper. Dishes were placed at room temperature in the dark. Four replicates of each treatment and the control (0 g/L – 5 mL of deionised water – dH_2O) were performed. Seed germination, defined as the seed having a radicle length > 5 mm [33], was evaluated every 12 h over a period of 7 days. The mean time to germination (MTG) of each plant species was calculated as follows:

$$MTG = \sum \frac{n \times d}{N} \quad (4)$$

where n is the number of seeds that germinated between each time period, d is the incubation period in minutes at that point and N is the total number of seeds that germinated in the treatment.

The germination index (GI) was determined for each species over a period of 48 h using the germination percentage and the radicle length:

$$\text{Germination index (GI\%)} = \frac{G_s}{G_c} \times \frac{L_s}{L_c} \times 100 \quad (5)$$

where Gs and Gc are the number of seeds that germinated in the sample and the control and Ls and Lc are the root lengths of the sample and the control, respectively. Germination index was measured as a percentage of control.

The germination studies data was analysed statistically using a One-way ANOVA (analysis of variance) to evaluate differences between the means of the different treatments. The Dunn's test was used to determine any significant differences ($p < 0.05$). ANOVA and Dunn's analyses were performed using SigmaPlot 13 (Sysstat, Chicago, IL).

3. Results

3.1. Swelling behaviour

The swelling capacity of the five nanocellulose superabsorbents was measured in deionised water as a function of time (Fig. 1). In general, all superabsorbents show a similar behaviour. After an initial absorption rate, swelling levels up to reach a plateau. The time required to reach maximum capacity ranged from a couple of hours, for freeze-dried superabsorbent, to 48 h for air-dried. Lyophilised superabsorbent is characterised by an initial rapid swelling with most of it occurring

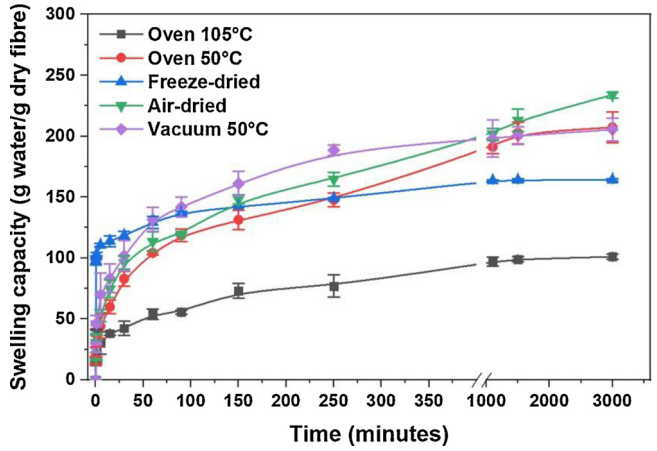

Fig. 1. Swelling capacity of nanocellulose superabsorbents produced using five different drying techniques as a function of time. Results are reported as mean ± standard deviation (n = 3).

during the first minutes. These results are consistent with literature on freeze-dried nanocellulose superabsorbents [6]. For the samples dried via evaporation, the swelling rate is slower. Both freeze-dried and vacuum-dried samples reached their equilibrium capacity within 5 h whereas oven-dried samples at low and high temperature achieved equilibrium after 24 h.

The absorption capacity at equilibrium of all samples was measured over time until constant mass was observed (Fig. 1). The swelling at equilibrium is a function of the drying rate employed, dictated by the drying technique. Surprisingly, in all cases- except for oven drying at 105 °C-, drying the nanocellulose by evaporation increased its equilibrium capacity over freeze-dried superabsorbents. Air-dried superabsorbent has the highest water absorption capacity at 230 g water/g dry fibre.

The rate of water removal as a function of time was measured for all the superabsorbents (Fig. 2). A direct relationship between the absorption capacity and the drying rate is observed. Among evaporative-dried superabsorbents, air-dried superabsorbents show the slowest drying followed by oven-dried 50 °C and vacuum-dried 50 °C. Oven-dried 105 °C superabsorbents display the fastest drying rate and also the lowest swelling capacity.

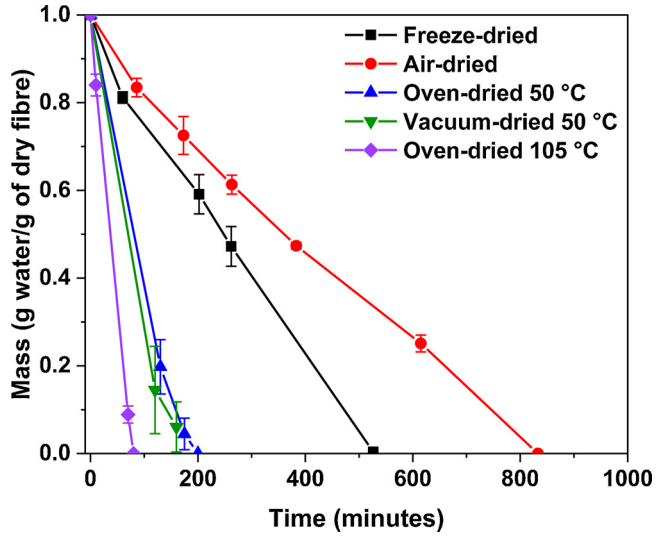

Fig. 2. Rate of water removal as a function of time of nanocellulose superabsorbents produced using five different drying techniques. Results are reported as mean ± standard deviation (n = 3).

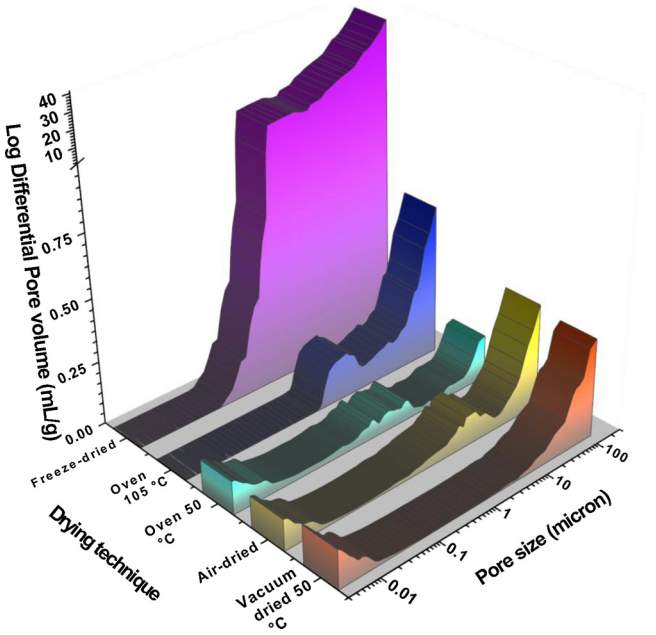

Fig. 3. Pore size distribution of nanocellulose superabsorbents using different drying techniques.

3.2. Pore size distribution

Mercury porosimetry was used to measure the pore size distribution of the nanocellulose superabsorbents prepared with the different drying techniques (Fig. 3). Pore size distribution notably changed depending on the drying mode categorized as freeze-drying or evaporative drying. Both freeze-dried superabsorbent and oven-dried 105 °C superabsorbent are characterised by a macroporous structure as defined by IUPAC [34] with no pores observed at a scale lower than 50 nm. Air-dried, oven-dried 50 °C and vacuum-dried 50°C superabsorbents all present a combination of macro, meso and micropores [34].

The relationship between bulk density, porosity, pore area (surface area) and volume of the superabsorbent is shown as a function of the drying technique in Fig. 4. Freeze-drying the nanocellulose superabsorbent produced an ultralight and highly porous material having a density lower than 170 kg/m^3 and a porosity higher than 90 %. These characteristics are typical of freeze-dried superabsorbents also referred to as nanocellulose foams [20]. In all cases, evaporative drying produced porous nanocellulose superabsorbents of porosities ranging from 50 to 60 % and with densities in between 1000 and 1400 kg/m^3. Vacuum-drying produced the superabsorbent of highest density (1400 kg/m^3). Freeze-drying and oven-drying at 105 °C produced superabsorbents with the lowest pore area. These values were around 7 times lower than with the other drying techniques. Freeze-dried nanocellulose superabsorbents have the highest pore volume: around 20 mL/g. This value is 60 times higher than for superabsorbents prepared through evaporative-drying.

3.3. Structure

To analyse the structural morphology of the superabsorbents, scanning electron microscopy (SEM) imaging was performed (Fig. 5). The visual appearance of each superabsorbent is shown in the supplementary information, S2. The morphology of the superabsorbents strongly depends on the drying rate. At low magnification, freeze-dried superabsorbent is characterised by a sheet-like network of fibres with interconnected pores of several microns in diameter. This morphology is typical of freeze-dried materials [20,24]. In contrast, evaporative-dried superabsorbents present a transparent film-like structure with no

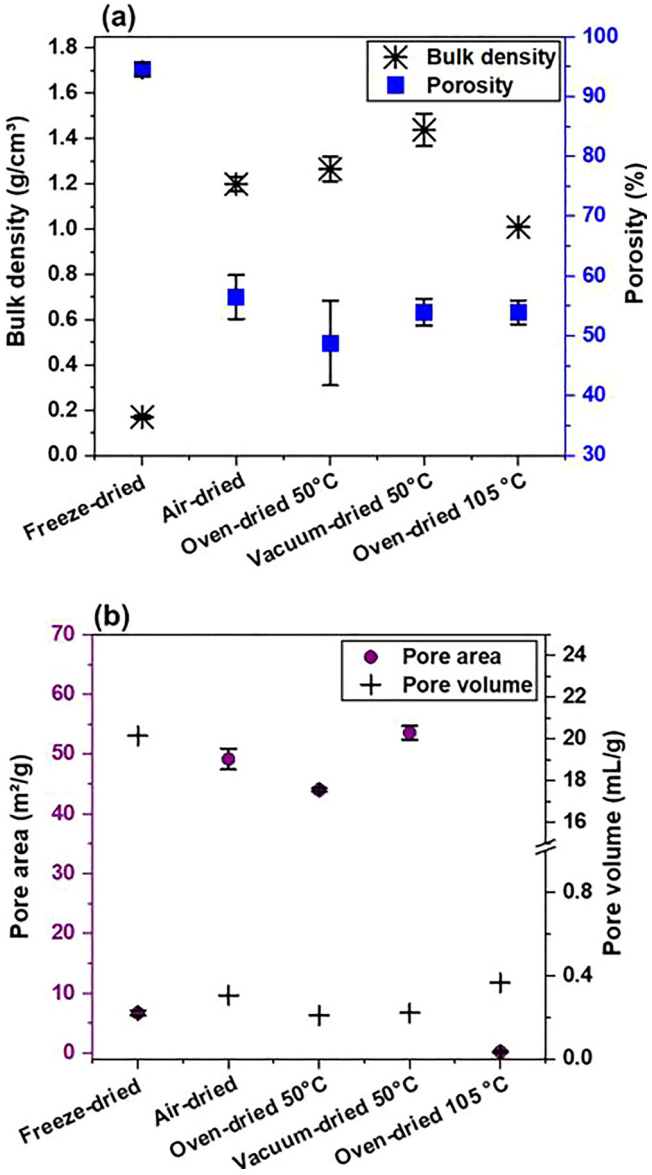

Fig. 4. (a) Porosity and bulk density of the different nanocellulose superabsorbents. (b) pore area and pore volume obtained through mercury porosimetry. Total porosity was calculated as: Total porosity $= .\left(\frac{pore\ volume}{skeletal\ volume\ +\ pore\ volume}\right) x\ 100\%$.

visible pores in the micrometre scale. For these, increasing the drying rate or temperature leads to an increase in surface roughness. Air-dried superabsorbent structure is homogeneous, soft and glassy whereas more micro-irregularities become evident as the temperature increases from 50 °C to 105 °C. These are due to fibre hornification which increases with temperature. At high magnification, freeze-dried superabsorbent forms a three-dimensional nanoporous network of fibres (Fig. 5a). The fibres are clearly visible and pore diameters range from 50 to 200 nm. The superabsorbents prepared by evaporation are characterised by two-dimensional structures of compact frames made of elemental entangled fibrils stacked on top of each other. Though the presence of small pores is observed in these cases, their diameter is difficult to measure by SEM due to the high density of fibres (Fig. 5b-d). The number of pores in oven-dried superabsorbent at 105 °C (Fig. 5e) is much lower than for the other evaporative-dried superabsorbents.

Small angle X-ray scattering (SAXS) was used to evaluate the pore structure and their distribution in the superabsorbents (Fig. 6). SAXS is a non -destructive method providing the morphology and distribution of nanoscale structures over a complete volume [35–37]. The pore structure and distribution of the superabsorbents are dependent on the drying technique. In SAXS, superabsorbents air-dried, oven-dried 50 °C and vacuum-dried 50 °C display a uniform isotropic scattering. The pore size distribution from the SAXS curves were obtained by modelling the scattering using the sphere shape model [38] combined with the log-normal pore distribution. The pore size distribution evaluated from SAXS curve fitting is similar to the pore distributions from mercury porosimetry (Fig. 6d). However, the SAXS images of freeze-dried and oven-dried 105 °C superabsorbents show anisotropic scattering (supplementary information, S3) revealing the pores are not distributed in a particular direction. In both cases, the pore sizes are large and beyond the size range measurement of lab SAXS setup.

3.4. Phytotoxicity assays

To determine the effect of the superabsorbents in plants, a germination experiment was conducted. Radish and cress seeds were treated with three different concentrations of 2 types of superabsorbents: freeze-dried and oven-dried 50 °C (to represent superabsorbents produced via evaporation). The mean time to germination (MTG) of both species is shown in Fig. 7. There was no significant difference in the MTG between the dH_2O control (0 g/L) and the freeze-dried or oven-dried 50 °C treatments. The MTG remains constant in all cases.

The germination index (GI) was calculated by measuring the radicle length of seeds grown on the superabsorbents for 48 h (Fig. 8). Radish and cress seeds grown over freeze-dried superabsorbent show no significant difference between the dH_2O control and any of the freeze-dried concentrations. Radish seeds treated with oven-dried 50 °C superabsorbent exhibit an increase in GI between the concentrations of 2–5 g/L (compared with the control). In contrast, a slight decrease in GI is observed in cress seeds treated with oven-dried 50 °C superabsorbent at the highest concentration of 10 g/L.

4. Discussion

4.1. Effect of drying rate on the superabsorbent structure and swelling rate

Nanocellulose-based superabsorbents of varying structures were prepared by adjusting the drying rate controlled with the drying mode. We raise the hypothesis that the rate of water removal from the hydrogel network controls its micro and nano structure. The effect of the structure on the swelling rate and superabsorption of nanocellulose was measured.

The structure of the superabsorbents was analysed by scanning electron microscopy (SEM), mercury porosimetry and small angle X-ray scattering (SAXS). While SEM provides three-dimensional and high-resolution images in a wide range of magnification, this technique is limited in quantifying material size and distribution [39]. Mercury porosimetry measures the pore size distribution which is used to calculate specific surface area and density. However, Hg porosiometry cannot quantify closed pores and measures the largest entrance of pores - not the actual inner size [40]. SAXS measurement generates the particle size, distribution and shape variations [37]. The combination of these three techniques can define the superabsorbent structure both at the micro and nanoscale with certainty.

Freeze-dried superabsorbent achieved the fastest absorption rate (Fig. 1). This is due to their high porosity with the network of fibres forming pores ranging from 50 nm to 100 µm. Kuśtrowski, et al. [41] also reported similar pore properties for fast-swelling polysaccharides superabsorbents. High porosity polymeric networks allow fast water diffusion across the superabsorbent [13]. In general, superabsorbents dried by evaporation have a much slower swelling rate, with around 10 % of their capacity reached during the first minutes.

Two distinct regimes are observed in the swelling kinetics of nanocellulose superabsorbents: (i) a steep initial uptake of water and (ii)

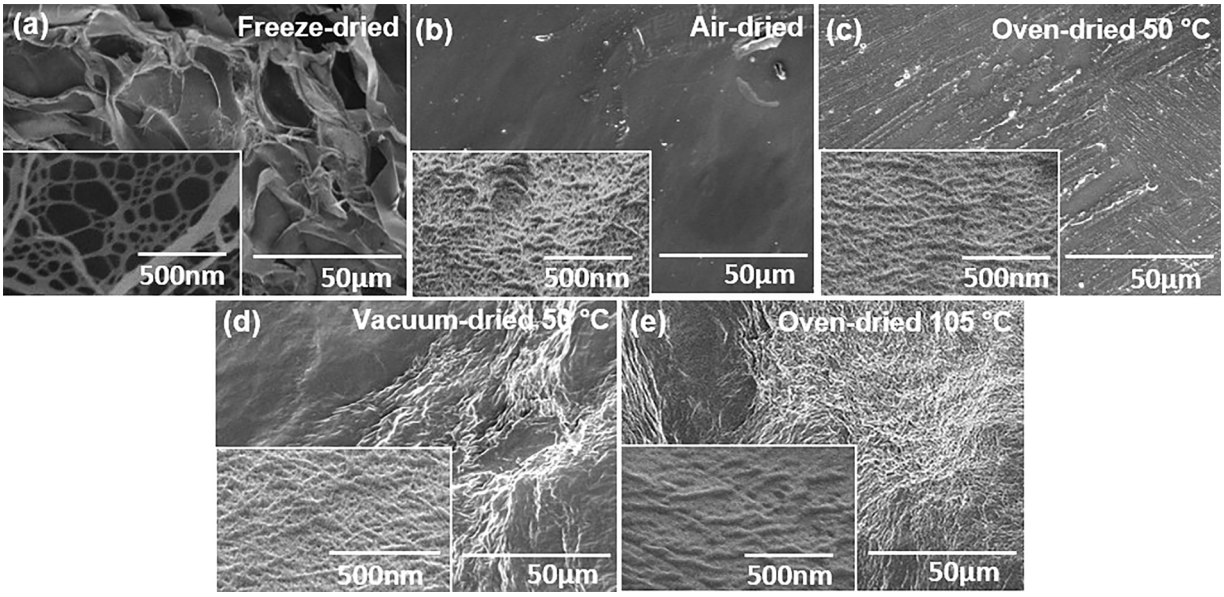

Fig. 5. SEM micrographs of the nanocellulose superabsorbent produced by changing the drying rate with the drying methods: (a) freeze-drying, (b) air-dried, (c) oven-dried at 50 °C, (d) vacuum oven-dried at 50 °C and (e) oven-dried 105 °C.

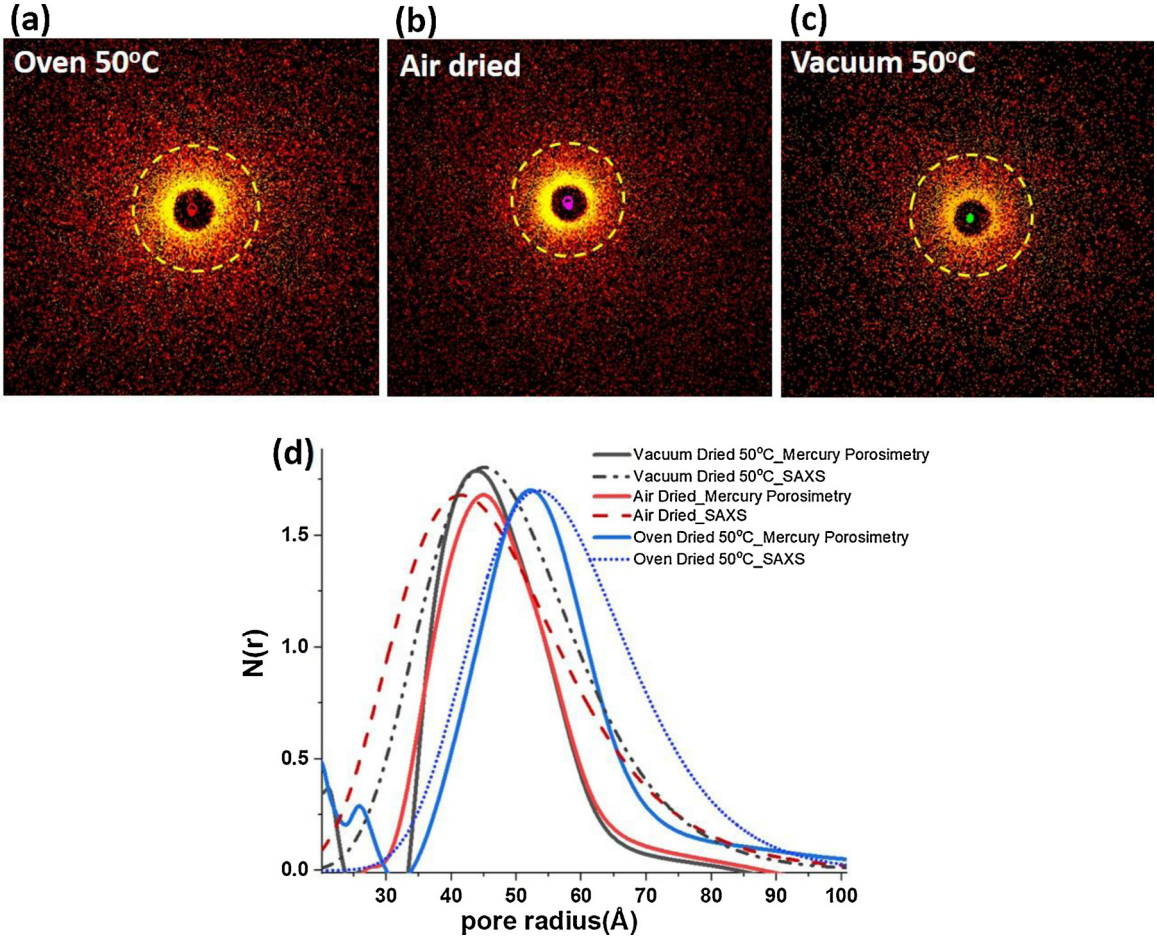

Fig. 6. Small angle X-ray scattering (SAXs) images of the nanocellulose superabsorbent produced at different drying rates: (a) air-dried, (b) oven-dried at 50 °C, (c) vacuum oven-dried at 50 °C. (d) Pore distribution of SAXs and mercury porosimetry tests. SAXS images of freeze-dried and oven-dried at 105 °C displayed in supporting information.

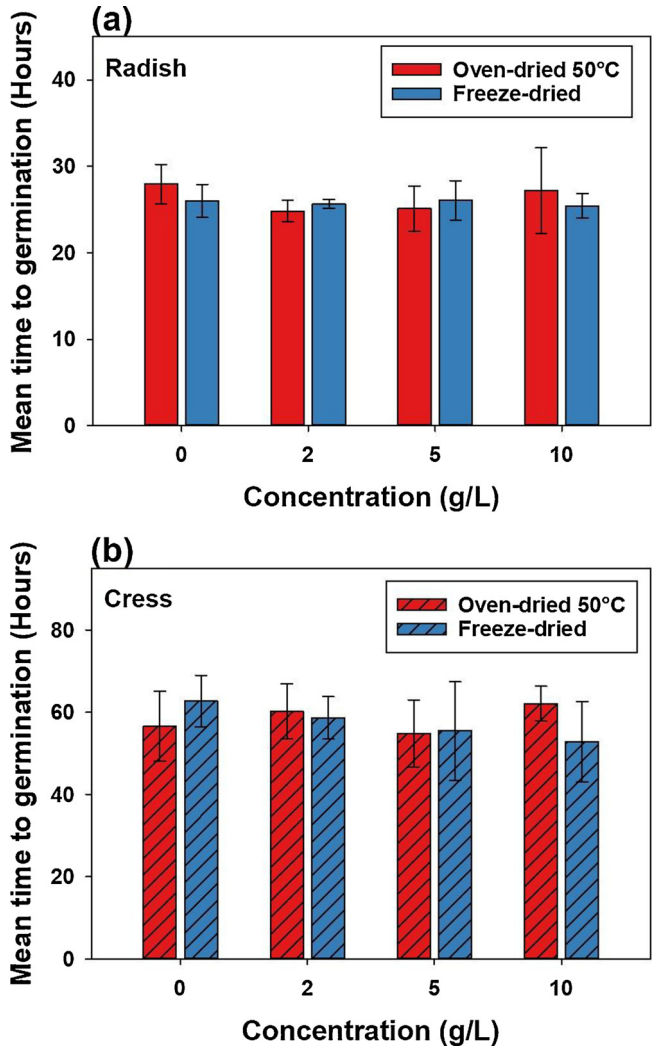

Fig. 7. Mean time to germination of (a) radish and (b) cress in the presence of increasing concentrations of two different types of superabsorbents: oven-dried 50 °C and freeze-dried. Results are reported as mean ± standard deviation (n = 4). Pictures of the phytotoxicity tests are shown in supplementary information, S4.

an asymptotical process towards the equilibrium swelling ratio. The effect of the drying technique on the swelling ratio was analysed using Schott's second-order kinetics model [42]

$$\frac{t}{Q_t} = \frac{1}{K_s Q_\infty^2} + \frac{1}{Q_\infty} t \quad (6)$$

where Q_∞ denotes the swelling capacity at equilibrium, K_s is the swelling rate constant, Q_t is the swelling capacity at time t. Because $K_{is} = K_s Q_\infty^2$, Eq. (6) can be expressed as:

$$\frac{t}{Q_t} = \frac{1}{K_{is}} + \frac{1}{Q_\infty} t \quad (7)$$

where K_{is} refers to the initial swelling rate constant [43]. Plots of the average swelling rate (t/Q_t) versus time (t) are displayed in Fig. 9; the expected straight lines are achieved ($R^2 > 0.99$) in all cases. This confirms that the swelling process follows a second-order kinetic model. This model successfully described semicrystalline polymers such as cellulose or gelatin [6,42,43].

The swelling kinetic parameters K_s, K_{is} and Q_∞ obtained from the slopes and intercepts of the plots (Fig. 9) are listed in Table 2 . The theoretical absorption capacity at equilibrium (Q_{theo}) is similar to the experimental absorption capacity (Q_{actual}) in all cases. Both the initial (K_{is}) and actual (K_s) swelling rate constants varied accordingly to the drying technique. K_{is} indicates the point where the buffer solution has permeated the entire film but before the polymer network stress relaxation retards swelling [42]. For freeze-dried superabsorbents, high porosity and pore size speed up the diffusion rate of water molecules into the superabsorbent, resulting in the highest K_{is}. In contrast, air-dried superabsorbents present a K_{is} around four times lower which indicates a slower diffusion rate of water molecules induced by the material porosity.

The swelling rate constant, K_s, is related to the solvent diffusion and relaxation process of the polymer chains [44]. Low values K_s suggest a rate controlled by stress relaxation in the swelling polymer network-not by diffusion-controlled swelling [42]. Air-dried superabsorbent presented the lowest K_s. The water molecules in this material diffused throughout the material during the first hour of immersion as shown by their soft and transparent appearance; however, equilibrium swelling was reached after 24 h. This indicates that the rate determining process is stress relaxation of the fibre network driven by the osmotic swelling pressure [42]. The same absorption mechanism applies to oven-dried at 50 °C and vacuum-dried at 50 °C. Freeze-dried superabsorbent reached saturation during the first minutes of experiment, suggesting a diffusion driven process. For the oven-dried superabsorbents at 105 °C, the swelling rate constant is higher than those from the other drying evaporation techniques. This indicates superabsorbent reaching saturation at a faster rate due to hornification, resulting in superabsorbents of smaller pores and inaccessible carboxylate groups, lowering swelling capacity.

4.2. Swelling capacity and water retention of nanocellulose superabsorbents

Two main variables are responsible for the superabsorption behaviour of nanocellulose. The first is porosity that enables diffusion of water molecules into the fibre network. This leads to the physical entrapment of water loosely held between nanofibres by capillary forces [6]. The second is the superabsorbent surface area. This facilitates the interaction between water and carboxylate groups (COO^-) and promotes hydrogen bonding. The fibre network expands and accommodates the influx of water through the relaxation of fibres driven by osmotic pressure [22,42]. The type of cations in the superabsorbent matrix also impacts water uptake [45]. However, only Na^+ was investigated in this study. Hence, the effects in the swelling capacity are directly related to the drying rate defining the structure of the superabsorbents.

Surprisingly, in all cases – except those dried at 105 °C – evaporative drying resulted in superabsorbents of higher swelling capacity than those produced by sublimation/freeze-drying. This contrasts from literature which reports that freeze-dried superabsorbent have higher absorption capacity than evaporative-dried superabsorbent [20,22,24,46]. This is because hornification in evaporative drying produces capillary pressure-induced stresses, shrinking pores and decreasing swelling capacity [24,25]. However, low-temperature drying and introducing anionic charges into the cellulose structure, such as carboxylate groups, minimise hornification of cellulose fibres [22,25,27]. These techniques were selected in our study.

Nevertheless, the high absorption capacity of our nanocellulose superabsorbents prepared by evaporative drying cannot be solely explained by the minimisation of hornification. Such performance is due to a combination of factors, all controlled by the drying rate. First, porosity and pore size enable physical entrapment of water into the superabsorbent network. This property is accentuated in freeze-dried superabsorbent having a porosity of > 90 %, which partly explains its absorption capacity [6]. The high absorption capacity of evaporative-dried superabsorbents is attributed largely to their high pore area higher than 45 m^2/g (Fig. 10). This increases the number of accessible COO^- groups participating in hydrogen bonding with water compared to freeze-dried superabsorbents, increasing the interaction of water

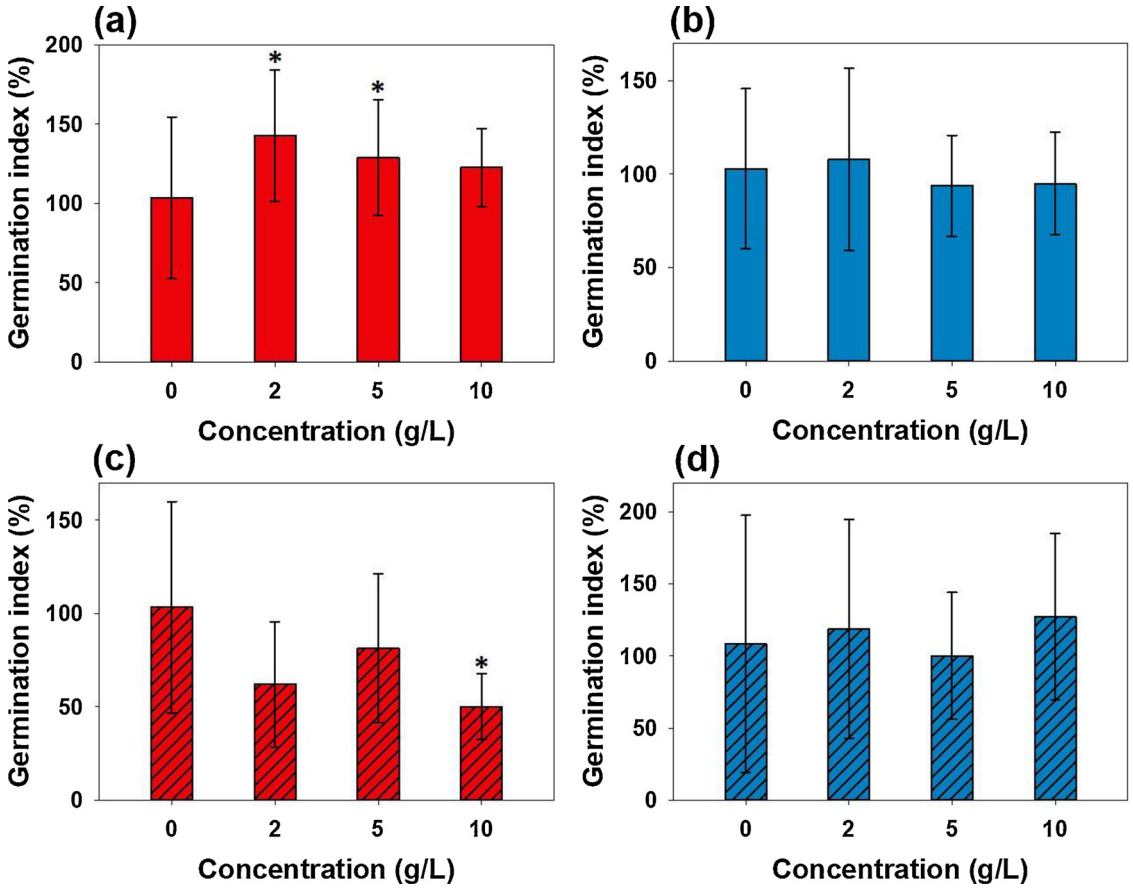

Fig. 8. Germination index of radish species treated with (a) oven-dried 50 °C and (b) freeze-dried superabsorbents, and cress species treated with (c) oven-dried 50 °C and (d) freeze-dried superabsorbents. Statistical difference according to ANOVA analysis followed by Dunn's test against 0 g/L concentration as control indicated as *P < 0.05, N = 4.

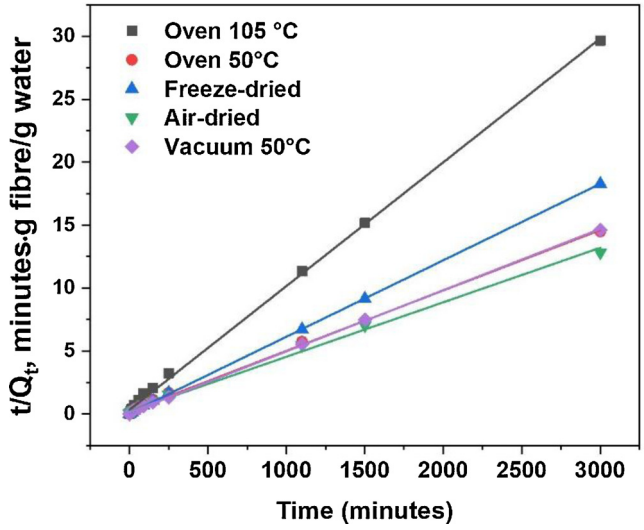

Fig. 9. Plots of t/Qt vs t according to Eq. 5 based on the experimental data displayed in Fig. 1.

adsorbed onto the polymer chains and swelling of the fibre network [47]. This, coupled with the pore size, lead to a stronger physical entrapment of water in between nanofibres by capillary forces.

These characteristics of evaporative-dried superabsorbents are given by rate of water removal. A relationship between this rate and the absorption capacity is observed. For these superabsorbents, Figs. 1 and 2 show that the slower the drying rate, the higher the absorption capacity achieved. This is because slow rates lead to a more uniform arrangement of fibres, producing superabsorbents with macro, meso and micropores which results in high absorption capacity.

Table II
Swelling kinetic parameters of the different superabsorbents.

Type	Qactual (g/g)	Qtheo (g/g)	Kis (g/g min)	Ks (10^{-5}, g/g min)
Oven-dried 105 °C	101.16	102.04	3.11	29.94
Oven-dried 50 °C	207.25	208.33	4.98	11.48
Freeze-dried	164.13	163.93	17.93	66.73
Air-dried	233.93	232.55	4.75	8.78
Vacuum 50 °C	205.43	204.08	9.95	23.91

These hypotheses are also supported by the water retention values (WRV) shown in Fig. 10. A relationship between the pore area and the WRV is observed. Evaporative dried superabsorbents – except for those oven-dried at 105 °C – exhibit high pore area and high-water retention properties, while freeze-dried superabsorbent shows low pore area and low WRV. This is attributed to the large pore size which promotes the release of water molecules from the superabsorbent matrix.

4.3. Importance of nanocellulose superabsorbent structure in agriculture

Seed germination is one of the most important phases in the life cycle of a plant and is highly dependent on the existing environment [48]. Seed germination bioassays and early stage seedling growth studies are commonly used for determining toxicity effects in plants. In the development of novel materials as growing media, the absence of phytotoxicity is the first requirement [11]. In this study, seed

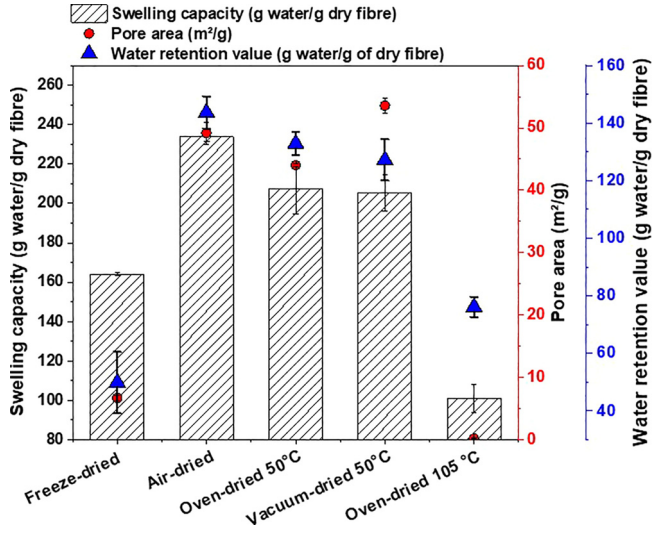

Fig. 10. Relationship between the drying technique, the swelling capacity, pore area and water retention value of nanocellulose superabsorbent.

germination and early stage seedling growth tests of radish and cress were conducted on two materials: freeze-dried and oven-dried 50 °C. The freeze-dried superabsorbent was chosen because of its difference in morphology compared to evaporative-dried superabsorbents, while oven-dried 50 °C was selected to represent superabsorbents dried via evaporation – the best condition for industrial scale production. Results show that any of the superabsorbents used in this study influenced the mean time to germination of either radish or cress seeds compared to the control (deionized water – dH_2O). This indicates that if seeds were to be grown in soil with nanocellulose superabsorbent, the time to emergence is unlikely to be affected, and hence its application in agriculture is safe for plants.

Moreover, radish seeds treated with oven-dried 50 °C exhibit an increase in the germination index by 30–40%. Such results are not observed in seeds treated with freeze-dried superabsorbent. This increase is attributed to the swelling kinetics of evaporative-dried superabsorbent being slower than freeze-dried superabsorbent, which increases the water availability at the early stage of seed germination. These positive effects confirm the results reported on superabsorbents improving seedling growth, regulating plants available water and reducing the detrimental effects produced by water stress [11,49].

5. Conclusion

A series of nanocellulose superabsorbents varying in pore properties was characterized in structure and swelling behaviour for application as hydro retentor in agriculture. Nanocellulose superabsorbent superabsorbents were prepared from TEMPO oxidized cellulose superabsorbents [6]. The structure of the nanocellulose superabsorbent was controlled with the drying rate of the superabsorbent. This was engineered with the drying process. Five methods, each providing a different rate of water removal, were studied. These include: freeze-dried, air-dried, vacuum-dried at 50 °C, and oven-dried at 50 °C and 105 °C. The effect of drying on the superabsorbent structure, swelling capacity, absorption rate, water retention and seed germination was analysed.

The structure of the nanocellulose superabsorbent, measured in terms of porosity, pore volume and area, is governed by the drying technique used. This structure directly impacts swelling capacity and kinetics. Freeze-dried superabsorbents are characterised by a three-dimensional macroporous network of fibres and pores ranging from 50 nm to 100 µm, whereas evaporative-dried superabsorbents form two-dimensional network of entangled fibrils stacked on top of each other. The high porosity and large pore size of freeze-dried superabsorbents are responsible for their fastest absorption rate. These superabsorbents exhibit a diffusion-controlled swelling mechanism. The absorption mechanism of evaporative-dried superabsorbents is dictated by stress relaxation of the fibre network. Both mechanisms are described by a second-order kinetics model [42]. Air-dried superabsorbents have the highest swelling capacity. This is attributed to pore area and strong water bond interaction. Superabsorbents oven-dried at 105 °C have the lowest swelling capacity due to fibre hornification [25].

Seed germination of radish and cress seeds demonstrates that the nanocellulose-based superabsorbents tested in this study are suitable for agricultural use; the SAP performance was independent of the drying process. This study identified evaporative drying as the best drying technique to produce high capacity superabsorbents. This technique is far easier and cheaper than freeze-drying, decreasing production costs of nanocellulose superabsorbents.

CRediT authorship contribution statement

Ruth M. Barajas-Ledesma: Conceptualization, Validation, Methodology, Investigation, Software, Writing - original draft. **Antonio F. Patti:** Supervision, Writing - review & editing. **Vanessa N.L. Wong:** Supervision, Writing - review & editing. **Vikram Singh Raghuwanshi:** Validation, Software, Writing - review & editing. **Gil Garnier:** Visualization, Supervision, Writing - review & editing.

Declaration of Competing Interest

The authors declare that they have no known competing financial interests or personal relationships that could have appeared to influence the work reported in this paper.

Acknowledgements

Many thanks to the Australian Research Council (ARC), Australian paper, Circa, Norske Skog, Orora, Visy and the Government of Tasmania, for financial support through the Industry Transformation Research Hub Processing Advance Lignocellulosics (PALS) grant IH130100016. Special thanks to the Monash Centre for Electron Microscopy for providing training and giving access to their facilities.

Appendix A. Supplementary data

Supplementary material related to this article can be found, in the online version, at doi:https://doi.org/10.1016/j.colsurfa.2020.124943.

References

[1] J.R. Gross, The evolution of absorbent materials, in: L. Brannon-Peppas, R.S. Harland (Eds.), Studies in Polymer Science, vol. 8, Elsevier, 1990, pp. 3–22.
[2] E.M. Ahmed, Hydrogel: preparation, characterization, and applications: a review, J. Adv. Res. 6 (2) (2015) 105–121, https://doi.org/10.1016/j.jare.2013.07.006.
[3] S. Ghorbani, et al., Hydrogels based on cellulose and its derivatives: applications, synthesis, and characteristics, Polym. Sci. Ser. A 60 (6) (2019) 707–722, https://doi.org/10.1134/s0965545x18060044.
[4] X. Shen, J.L. Shamshina, P. Berton, G. Gurau, R.D. Rogers, Hydrogels based on cellulose and chitin: fabrication, properties, and applications, Green Chem. 18 (1) (2016) 53–75, https://doi.org/10.1039/C5GC02396C.
[5] R. Curvello, V.S. Raghuwanshi, G. Garnier, Engineering nanocellulose hydrogels for biomedical applications, Adv. Colloid Interface Sci. 267 (2019) 47–61, https://doi.org/10.1016/j.cis.2019.03.002.
[6] L. Mendoza, L. Hossain, E. Downey, C. Scales, W. Batchelor, G. Garnier, Carboxylated nanocellulose foams as superabsorbents, J. Colloid Interface Sci. 538 (March) (2019) 433–439, https://doi.org/10.1016/j.jcis.2018.11.112.
[7] H.M. Shewan, J.R. Stokes, Review of techniques to manufacture micro-hydrogel particles for the food industry and their applications, J. Food Eng. 119 (4) (2013) 781–792, https://doi.org/10.1016/j.jfoodeng.2013.06.046.
[8] A. Bashari, A. Rouhani Shirvan, M. Shakeri, Cellulose-based hydrogels for personal care products, Polym. Adv. Technol. 29 (12) (2018) 2853–2867, https://doi.org/10.1002/pat.4290.
[9] S. Basak, N. Nandi, S. Paul, I.W. Hamley, A. Banerjee, A tripeptide-based self-shrinking hydrogel for waste-water treatment: removal of toxic organic dyes and

lead (Pb2+) ions, Chem. Commun. 53 (43) (2017) 5910–5913, https://doi.org/10.1039/C7CC01774J.
[10] T.M. Neethu, P.K. Dubey, A.R. Kaswala, Prospects and applications of hydrogel technology in agriculture, Int. J. Curr. Microbiol. Appl. Sci. 7 (05) (2018) 3155–3162, https://doi.org/10.20546/ijcmas.2018.705.369.
[11] F.F. Montesano, A. Parente, P. Santamaria, A. Sannino, F. Serio, Biodegradable Superabsorbent Hydrogel Increases Water Retention Properties of Growing Media and Plant Growth, Agric. Agric. Sci. Procedia 4 (2015) 451–458, https://doi.org/10.1016/j.aaspro.2015.03.052.
[12] M.J. Zohuriaan-Mehr, Kourosh Kabiri, Superabsorbent polymer materials: a review, Iran. Polym. J. 17 (6) (2008) 451–477.
[13] M.R. Guilherme, et al., Superabsorbent hydrogels based on polysaccharides for application in agriculture as soil conditioner and nutrient carrier: a review, Eur. Polym. J. 72 (2015) 365–385, https://doi.org/10.1016/j.eurpolymj.2015.04.017.
[14] M.R. Guilherme, A.V. Reis, A.T. Paulino, T.A. Moia, L.H.C. Mattoso, E.B. Tambourgi, Pectin-based polymer hydrogel as a carrier for release of agricultural nutrients and removal of heavy metals from wastewater, J. Appl. Polym. Sci. (2010), https://doi.org/10.1002/app.32123 pp. n/a-n/a.
[15] J. Zhang, L. Wang, A. Wang, Preparation and swelling behavior of fast-swelling superabsorbent hydrogels based on starch-g-poly(acrylic acid-co-sodium acrylate), Macromol. Mater. Eng. 291 (6) (2006) 612–620, https://doi.org/10.1002/mame.200500387.
[16] S. Varanasi, R. He, W. Batchelor, Estimation of cellulose nanofibre aspect ratio from measurements of fibre suspension gel point, Cellulose 20 (4) (2013) 1885–1896, https://doi.org/10.1007/s10570-013-9972-9.
[17] S.M.F. Kabir, P.P. Sikdar, B. Haque, M.A.R. Bhuiyan, A. Ali, M.N. Islam, Cellulose-based hydrogel materials: chemistry, properties and their prospective applications, Prog. Biomater. 7 (September (3)) (2018) 153–174, https://doi.org/10.1007/s40204-018-0095-0.
[18] Q. Li, S. McGinnis, C. Sydnor, A. Wong, S. Renneckar, Nanocellulose Life Cycle Assessment, ACS Sustain. Chem. Eng. 1 (8) (2013) 919–928, https://doi.org/10.1021/sc4000225.
[19] A. Isogai, T. Saito, H. Fukuzumi, TEMPO-oxidized cellulose nanofibers, Nanoscale 3 (1) (2011) 71–85, https://doi.org/10.1039/C0NR00583E.
[20] N. Lavoine, L. Bergström, Nanocellulose-based foams and aerogels: processing, properties, and applications, J. Mater. Chem. A 5 (31) (2017) 16105–16117, https://doi.org/10.1039/c7ta02807e.
[21] K.J. De France, T. Hoare, E.D. Cranston, Review of Hydrogels and Aerogels Containing Nanocellulose, Chem. Mater. 29 (11) (2017) 4609–4631, https://doi.org/10.1021/acs.chemmater.7b00531.
[22] I.H. Mondal, Cellulose-Based Superabsorbent Hydrogels (Polymers and Polymeric Composites: A Reference Series), (2019).
[23] Z. Pakowski, Modern methods of drying nanomaterials, Transp. Porous Media 66 (1–2) (2006) 19–27, https://doi.org/10.1007/s11242-006-9019-x.
[24] N. Buchtová, T. Budtova, Cellulose aero-, cryo- and xerogels: towards understanding of morphology control, Cellulose 23 (August (4)) (2016) 2585–2595, https://doi.org/10.1007/s10570-016-0960-8.
[25] M. Beaumont, J. König, M. Opietnik, A. Potthast, T. Rosenau, Drying of a cellulose II gel: effect of physical modification and redispersibility in water, Cellulose 24 (3) (2017) 1199–1209, https://doi.org/10.1007/s10570-016-1166-9.
[26] N. Butchosa, Q. Zhou, Water redispersible cellulose nanofibrils adsorbed with carboxymethyl cellulose, Cellulose 21 (December (6)) (2014) 4349–4358, https://doi.org/10.1007/s10570-014-0452-7.
[27] T. Lindstrom, G. Carlsson, The effect of carboxyl groups and their ionic form during drying on the hornification of cellulose fibers, svensk papperstidning (1982) R146.
[28] S. Ang, V. Haritos, W. Batchelor, Cellulose nanofibers from recycled and virgin wood pulp: a comparative study of fiber development, Carbohydr. Polym. 234 (2020) 115900, https://doi.org/10.1016/j.carbpol.2020.115900.
[29] T. Saito, A. Isogai, TEMPO-Mediated Oxidation of Native Cellulose. The Effect of Oxidation Conditions on Chemical and Crystal Structures of the Water-Insoluble Fractions, Biomacromolecules 5 (5) (2004) 1983–1989, https://doi.org/10.1021/bm0497769.
[30] Urine-absorbing aids for incontinence - Test methods for characterizing polymer-based absorbent materials ISO 17190-17196, Geneva, 2001.
[31] J.W. Qingzheng Cheng, Joseph F. McNeel, Peter M. Jacobson, Water retention value measurements of cellulosic materials using a centrifuge technique, BioResources 5 (3) (2010) 1945–1954.
[32] S. Karnani, Viji, Hydrogel Agriculture Technology (Accessed 06 February 2020), http://vikaspedia.in/agriculture/best-practices/sustainable-agriculture/crop-management/hydrogel-agriculture-technology.
[33] K.P. Mosse, A.F. Patti, E.W. Christen, T.R. Cavagnaro, Winery wastewater inhibits seed germination and vegetative growth of common crop species, J. Hazard. Mater. 180 (August (1–3)) (2010) 63–70, https://doi.org/10.1016/j.jhazmat.2010.02.069.
[34] IUPAC, Compendium of Chemical Terminology, 2nd ed. (the "Gold Book"), Blackwell Scientific Publications, Oxford, 1997.
[35] V.S. Raghuwanshi, et al., Cationic polyacrylamide induced nanoparticles assembly in a cellulose nanofiber network, J. Colloid Interface Sci. 529 (2018) 180–186, https://doi.org/10.1016/j.jcis.2018.06.009.
[36] V.S. Raghuwanshi, U.M. Garusinghe, J. Ilavsky, W.J. Batchelor, G. Garnier, Effect of nanoparticles size and polyelectrolyte on nanoparticles aggregation in a cellulose fibrous matrix, J. Colloid Interface Sci. 510 (2018) 190–198, https://doi.org/10.1016/j.jcis.2017.09.064.
[37] O. Glatter, O. Kratky, Small Angle X-Ray Scattering, Academic Press, London, New York, 1982.
[38] V.S. Raghuwanshi, M. Ochmann, F. Polzer, A. Hoell, K. Rademann, Self-assembly of gold nanoparticles on deep eutectic solvent (DES) surfaces, Chem. Commun. 50 (63) (2014) 8693–8696, https://doi.org/10.1039/C4CC02588A.
[39] L.C. Gomes, J.M.R. Moreira, M. Simões, L.F. Melo, F.J. Mergulhão, Biofilm localization in the vertical wall of shaking 96-well plates (in eng), Scientifica (Cairo) 2014 (2014) 231083, https://doi.org/10.1155/2014/231083.
[40] H. Giesche, Mercury porosimetry: a general (practical) overview, Part. Part. Syst. Charact. 23 (1) (2006) 9–19, https://doi.org/10.1002/ppsc.200601009.
[41] P. Kuśtrowski, P. Natkański, A. Rokicińska, and E. Witek, Polymer Hydrogel-Clay (Nano) Composites in Polymer Gels, (Gels Horizons: From Science to Smart Materials, 2018, Chapter 1, pp. 1–62.
[42] H. Schott, Swelling kinetics of polymers, J. Macromol. Sci. Part B- Phys. 31 (1) (2006) 1–9, https://doi.org/10.1080/00222349208215453.
[43] X. Shi, W. Wang, A. Wang, pH-responsive sodium alginate-based superporous hydrogel generated by an anionic surfactant micelle templating, Carbohydr. Polym. 94 (1) (2013) 449–455, https://doi.org/10.1016/j.carbpol.2013.01.019.
[44] F. Rosa, J. Bordado, M. Casquilho, Kinetics of water absorbency in AA/AMPS copolymers: applications of a diffusion–relaxation model, Polymer 43 (1) (2002) 63–70, https://doi.org/10.1016/S0032-3861(01)00596-1.
[45] I. Homma, H. Fukuzumi, T. Saito, A. Isogai, Effects of carboxyl-group counter-ions on biodegradation behaviors of TEMPO-oxidized cellulose fibers and nanofibril films, Cellulose 20 (5) (2013) 2505–2515, https://doi.org/10.1007/s10570-013-0020-6.
[46] J. Nemoto, T. Soyama, T. Saito, A. Isogai, Nanoporous networks prepared by simple air drying of aqueous TEMPO-oxidized cellulose nanofibril dispersions, Biomacromolecules 13 (March (3)) (2012) 943–946, https://doi.org/10.1021/bm300041k.
[47] Z. Xia, M. Patchan, J. Maranchi, J. Elisseeff, M. Trexler, Determination of cross-linking density of hydrogels prepared from microcrystalline cellulose, J. Appl. Polym. Sci. 127 (6) (2013) 4537–4541, https://doi.org/10.1002/app.38052.
[48] A.G. Rombola, et al., Relationships between chemical characteristics and phytotoxicity of biochar from poultry litter pyrolysis, J. Agric. Food Chem. 63 (August (30)) (2015) 6660–6667, https://doi.org/10.1021/acs.jafc.5b01540.
[49] M.K. Akhter, K.A. Malik, A. Mardan, M. Ahmad, M.M. Iqbal, Effects of hydrogel amendment on water storage of sandy loam and loam soils and seedling growth of barley, wheat and chickpea, Plant Soil Environ. 50 (10) (2004) 463–469.